TOMOGRAPHIC SAR IMAGING OF A FORESTED AREA BY TIME-DOMAIN BACK-PROJECTION

Othmar Frey, Felix Morsdorf, Erich Meier

Remote Sensing Laboratories RSL, University of Zurich
Winterthurerstrasse 190, CH-8057 Zurich, Switzerland
ofrey@geo.unizh.ch

KEY WORDS: SAR, multi-baseline SAR, tomography, time-domain, back-projection, forest, vegetation

ABSTRACT:

Recently, various attempts have been undertaken to retrieve information about the three-dimensional structure of vegetation from multi-baseline synthetic aperture radar data. Although tomographic processing of such data has been demonstrated, yet, there are still several problems that limit the focusing quality. In particular, the frequency-domain based focusing methods are susceptible to irregular and sparse sampling, two problems, which are unavoidable in case of multi-pass, multi-baseline radar data acquired by an airborne system. We propose a time-domain back-projection algorithm, which maintains the original geometric relationship between the original sensor positions and the imaged target and is therefore able to cope with irregular and sparse sampling without introducing any geometric approximations. Preliminary results obtained with a newly acquired P-band tomographic data set consisting of eleven flight tracks are shown and discussed.

1 INTRODUCTION

In a conventional synthetic aperture radar (SAR) image multiple back-scattering elements distributed along the elevation component are projected to the two-dimensional slant-range plane. With Pol-InSAR techniques only a very limited number of different scattering elements can be localized within a resolution cell. Tomographic processing of SAR data, however, allows resolving the ambiguity in the elevation component and is therefore suitable to produce true three-dimensional images. Hence, different back-scattering elements within a volume can directly be localized. This property can be exploited for the reconstruction of volumetric structures, such as forested areas, as well as for a more detailed imaging of built-up areas and mountainous regions, which exhibit a high percentage of layover regions. Tomographic processing of SAR data requires that the synthetic aperture in azimuth be extended by a second dimension in direction orthogonal to the plane spanned by the vectors in azimuth and the line of sight. The sampling in this direction, called the normal direction, is realized by coherently combining a sufficient number of adequately separated flight paths.

A critical issue with respect to processing SAR data tomographically is that the common Fourier-based SAR processing algorithm, the SPECAN (SPECtral ANalysis) approach, which has been used by (Reigber and Moreira, 2000), requires a regular sampling spacing as well as a densely sampled synthetic aperture. In reality, the sampling spacing is not uniform at all when dealing with airborne SAR data of multiple acquisition paths, and, in addition, the synthetic aperture in the normal direction is sampled sparsely. Therefore these reconstruction approaches are prone to artifacts and defocusing in the final tomographic image. In order to overcome these problems modern spectral estimation methods have been proposed including spectral estimation by the Capon method (Lombardini and Reigber, 2003) and subspace-based spectral estimation such as MUSIC (Guillaso and Reigber, 2005), (Gini and Lombardini, 2005). But, since these methods only replace the last step, the spectral estimation, they still involve the geometric approximations made beforehand.

We adopt a time-domain back-projection (TDBP) processing technique, which maintains the entire three-dimensional geometric relationship between the exact sensor positions and the illuminated area while focusing the data. The key feature of the TDBP approach is an accurate handling of the complex geometry of irregularly spaced and sparsely sampled airborne SAR data.

In the next section, the Fourier-based SPECAN approach is revised in order to highlight the approximations that are involved. The same framework is also used to derive the sampling constraints and the spatial resolution for data processing in the normal direction. Then, the formulation of the TDBP algorithm for tomographic processing is presented. Further, we describe the measurement set-up of a tomographic SAR experiment and present preliminary results obtained from the TDBP-based tomographic reconstruction of a forested area from E-SAR P-band data.

2 THE SPECAN ALGORITHM, SPATIAL RESOLUTION AND SAMPLING SPACING IN THE NORMAL DIRECTION

For the first demonstration of airborne SAR tomography (Reigber and Moreira, 2000) the three-dimensional focusing of the data was accomplished by a combination of the extended chirp scaling algorithm (Moreira and Huang, 1994), which was used to focus each data track in range and azimuth direction, and the SPECAN algorithm, which was applied to focus the data in the normal direction. The SPECAN approach was originally designed for azimuth compression of ScanSAR data. The peculiarity of this algorithm lies in the fact that the focused data is obtained by a Fourier transform after a deramping operation.

We want to look again in some detail at the derivation of the SPECAN algorithm for focusing in the normal direction for two reasons: first, to highlight the approximations that are involved in the SPECAN approach, and second, because it provides a good framework to derive two important parameters, the *spatial resolution* δ_n and the *Nyquist sampling spacing* d_n in the normal direction.

The model that is used to derive these parameters follows to a large extent the derivation presented in (Reigber and Moreira,

2000). However, the signal model is loosely based on the derivation of the SPECAN algorithm for azimuth focusing as it is presented in (Cumming and Wong, 2005).

The simplified tomographic acquisition geometry that forms the basis for the derivation of the spatial resolution and the sampling constraints in normal direction n – i.e. orthogonal to the plane spanned by the slant-range direction and the azimuth direction – is depicted in Fig. 1. r_0 is the range distance at the point of closest approach along the synthetic aperture in normal direction n. Equally spaced baselines d_n are assumed and the variation of the off-nadir angle is neglected, so, the vector $\vec{n}$ in normal direction is assumed to be invariant for all acquisition paths. Target coordinates are identified by a bar above the symbol. Assuming

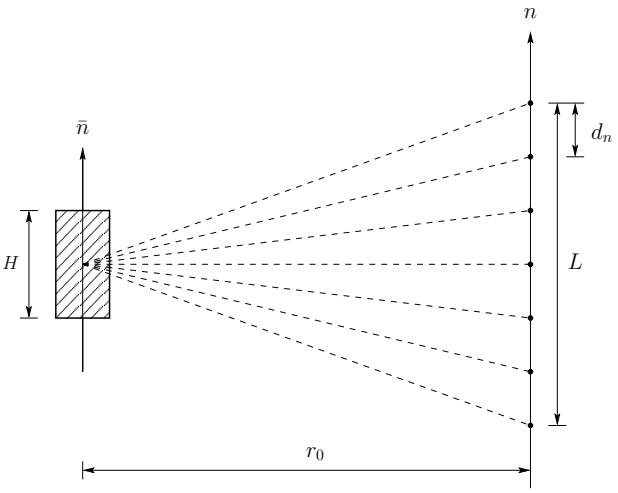

Figure 1: Simplified tomographic imaging geometry after (Reigber and Moreira, 2000). A volume is illuminated from different positions along a synthetic aperture in normal direction n. Each position in normal direction corresponds to a sensor path in azimuth direction. The sensor paths are separated by a constant sampling spacing d_n. The maximal height of the volume is H. L is the length of the synthetic aperture in normal direction.

that the synthetic aperture in the normal direction n is continuous - imagine an infinite number of single look complex images, represented by s_r, acquired from an infinite number of different, parallel flight tracks along n - the focused signal in normal direction $v(\bar{n}_0)$ at position $\bar{n}_0$ in the object space can be written as the following convolution in the time domain:

$$v(\bar{n}_0) = \int_{-L/2}^{L/2} s_r(\bar{n}_0 - n) h(n) dn \tag{1}$$

This is equivalent to:

$$v(\bar{n}_0) = \int_{\bar{n}_0 - L/2}^{\bar{n}_0 + L/2} s_r(n) h(\bar{n}_0 - n) dn \tag{2}$$

L is the length of the synthetic aperture in normal direction n. s_r is the demodulated, received signal. h is the matched filter, i.e. the time-reversed reference function, which can be written as:

$$h(\bar{n}_0 - n) = \exp\left(\frac{ik}{r_0}(\bar{n}_0 - n)^2\right) \tag{3}$$

This formulation implements a quadratic phase history, which is obtained by approximating the hyperbolic range history by a second order Taylor series expansion about the point $n = \bar{n}_0$:

$$r(n, \bar{n}_0) = 2\sqrt{r_0^2 + (\bar{n}_0 - n)^2} \simeq 2r_0 + \frac{(\bar{n}_0 - n)^2}{r_0} . \tag{4}$$

$r(n, \bar{n}_0)$ is the two-way path length between the sensor at position n and a back-scatterer within the observed volume at height $\bar{n}_0$, with a range distance r_0 at the point of closest approach. Inserting eq. (3) into eq. (2) and expanding the quadratic phase term yields:

$$v(\bar{n}_0) = \exp\left(\frac{ik}{r_0}\bar{n}_0^2\right) \cdot \int_{\bar{n}_0 - L/2}^{\bar{n}_0 + L/2} \underbrace{s_r(n) \exp\left(\frac{ik}{r_0} n^2\right)}_{s_d(n)} \exp\left(-\frac{i2k}{r_0}\bar{n}_0 n\right) dn . \tag{5}$$

The exponential within the underbraced term in eq. (5) can be interpreted as a deramping operation which leads to the deramped signal s_d. Then, the whole integral is equivalent to a Fourier transform of the deramped signal s_d:

$$v(\bar{n}_0) = \exp\left(\frac{ik}{r_0}\bar{n}_0^2\right) \int_{\bar{n}_0 - L/2}^{\bar{n}_0 + L/2} s_d(n) \exp\left(-\frac{i2k}{r_0}\bar{n}_0 n\right) dn . \tag{6}$$

So, in practise, the focused image $v(\bar{n}_0)$ can be obtained by applying a FFT to the deramped signal s_d.

The phase term in the exponent of eq. (6) can be written as:

$$-\frac{2k}{r_0}\bar{n}_0 n = -K_{nr}\bar{n}_0 n \tag{7}$$

where $K_{nr} = \frac{2k}{r_0}$ is interpreted as the spatial frequency modulation rate of the signal in normal direction. As it is well known from pulse compression of linear FM signals in range direction, the resolution in the time domain after compression is given by the reciprocal of the processed bandwidth, which is the product of the FM rate and the integration time. Translated to the normal direction and expressed in the spatial domain, the spatial resolution δ_n is the inverse of the product of the spatial frequency modulation rate K_{nr} and the integration path L times 2π:

$$\delta_n = \frac{2\pi}{K_{nr} \cdot L} = \frac{2\pi}{\frac{2 \cdot 2\pi}{r_0 \lambda} \cdot L} = \frac{\lambda r_0}{2L} . \tag{8}$$

The Nyquist sampling spacing d_n in normal direction is equivalent to the inverse of the spatial bandwidth k_n times 2π, where $k_n(\bar{n}_0) = K_{nr} \cdot \bar{n}_0 = \frac{2k}{r_0}\bar{n}_0$:

$$d_n(\bar{n}_0) \leq \left|\frac{2\pi}{k_n(\bar{n}_0)}\right| = \frac{2\pi}{K_{nr} \cdot \bar{n}_0} = \frac{\lambda r_0}{2\bar{n}_0} . \tag{9}$$

Eq. (9) describes the relationship between sampling spacing and the maximal height $\bar{n}_0 = H$ of the imaged volume that can be reconstructed unambiguously:

$$d_n(\bar{n}_0 = H) \leq \frac{\lambda r_0}{2H} . \tag{10}$$

3 3D FOCUSING IN THE TIME-DOMAIN

In (Nannini and Scheiber, 2006) an algorithm has been proposed which is also based on single look complex images processed by the extended chirp scaling algorithm including aircraft motion compensation to a straight line. However, instead of focusing the data by deramping and spectral estimation, which would

previously involve generating synthetic tracks followed by a regularization of the samples in the normal direction, a time-domain beamformer (TDB) was applied to focus the data in the third dimension. Every voxel within the volume is focused by a so-called *ad hoc* reference function as it is also known from time-domain back-projection processing. The focusing quality of the TDB approach was found to be superior to the SPECAN based algorithm presented in (Reigber and Moreira, 2000) for unevenly spaced baselines. But in spite of the fact that the TDB directly accounts for the irregular track distribution in normal direction it is still based on artificial, linearized flight tracks, which lie in parallel to each other and which do not represent the true geometry of the flight tracks.

We aim at a complete processing in the time domain – after range compression – and focus the data by using the true geometry of the irregularly sampled tomographic acquisition pattern. Our TDBP processor, which has been tested with airborne (Frey et al., 2006) and spaceborne SAR data (Frey et al., 2005), is extended in order to work with an irregularly sampled, two-dimensional synthetic aperture. Actually, the extension is a very natural one in the way that the signal contributions are not only combined along the flight path but are also coherently added along the normal direction. The main point is that the geometric relationship between every sensor position and the illuminated volume is maintained during focusing without introducing any geometric approximations.

Following the derivations presented in (Frey et al., 2005) the back-projected signal s_k corresponding to the flight track k can be expressed as a function of the grid point $\vec{r}_i$:

$$s_k(\vec{r}_i) = \sum_{j=a_k(\vec{r}_i)}^{b_k(\vec{r}_i)} g_k(R_k, \vec{r}_{S_{jk}}) \cdot R_k \cdot \exp(i2k_c R_k) \; . \quad (11)$$

$\vec{r}_i$	: position vector of the target
a_k, b_k	: indices of first, last azimuth position of the sensor within the synthetic aperture of the target position $\vec{r}_i$
$\vec{r}_{S_{jk}}$	: position vector of the sensor, $j \in [a_k, b_k]$
R_k	$= \lvert\vec{r}_i - \vec{r}_{S_{jk}}\rvert$: range distance
$g_k(.)$	: range-compressed signal of data track k
k_c	= $2\pi f_c/c$: central wavenumber
f_c	: carrier frequency
c	: speed of light

By extending the coherent addition of the signal contributions to the normal direction the back-projected signal v is obtained, which maps the volume at the position $\vec{r}_i$:

$$v(\vec{r}_i) = \sum_{k=1}^{m} \sum_{j=a_k(\vec{r}_i)}^{b_k(\vec{r}_i)} g_k(R_k, \vec{r}_{S_{jk}}) \cdot R_k \cdot \exp(i2k_c R_k) \; , \quad (12)$$

where m is the number of flight tracks that build the tomographic pattern. The boundaries of the synthetic aperture in azimuth direction, a_k and b_k, vary as a function of the grid position $\vec{r}_i$. This means that we sum up the contributions from those sensor positions $\vec{r}_{S_{jk}}$ which actually build the synthetic aperture for the grid position $\vec{r}_i$. Note that an appropriate interpolation procedure is required in order to retrieve the data values at the correct range distances because of the discrete representation of the range-compressed data.

4 EXPERIMENTAL SET-UP

An extensive airborne SAR campaign has been carried out in September 2006. Two fully polarimetric tomographic data sets - an L-band and a P-band data set - of a partially forested area have been acquired by the German Aerospace Center's E-SAR system. Eight corner reflectors were deployed for geometric and radiometric calibration purposes. The positions of the corner reflectors were measured by carrier-phase differential GPS. Several ground truth data are available: Four plots each of which consisting of nine accurately positioned hemispherical photographs have been sampled. The camera positions were measured with the help of a Leica total station to an absolute positioning accuracy lower than 10 cm. A digital elevation model (DEM) derived from airborne laser scanning (Falcon II, Toposys GmbH) is available for comparison of the ground level and a digital surface model (DSM) acquired by the same sensor is also at hand. However, the DSM is of limited value in terms of indicating forested areas because it stems from an campaign in early spring of 2003. So, besides the long time span as a limiting factor, it must also be assumed that the deciduous trees were mostly transparent to the laser signal and therefore do not appear in the DSM.

In Table 1 the system parameters of the E-SAR system are summarized. Note that the reduced chirp bandwidth of only 70 MHz in the P-band is due to restrictions imposed by the Swiss Federal Office of Communications to prevent interference of the radar signal with existing RF communication services within the band 390-395 MHz. The nominal chirp bandwidth is 94 MHz for both L- and P-band. The 12 P-band data sets were acquired within

	P-band	**L-band**
Carrier frequency	350 MHz	1.3 GHz
Chirp bandwidth	70 MHz	94 MHz
Sampling rate	100 MHz	100 MHz
Polarizations	HH-HV-VV-VH	HH-HV-VV-VH
PRF	500 Hz	400 Hz
Ground speed	90 m/s	90 m/s

Table 1: E-SAR system parameters.

one air mission. The maximal time span between the first and the last track is approx. 2 h. Due to mission duration constraints the 17 L-band tracks had to be shared among 2 missions resulting in a longer maximal time span of approximately 4.5 h between the first track of the first mission and the ultimate track of the second mission. The tracks of each tomographic pattern were flown in an interleaved manner in case that an unexpected incidence would have caused an untimely abortion of the data acquisition. In Fig. 2 and Fig. 3, respectively, the geometric configurations of the actual flight tracks for both tomographic data sets, P- as well as L-band, are shown. The flight direction is from east to west and the sensor is left-looking. In addition to the actual flight tracks, their projections to the horizontal plane and to the northing-height plane are also depicted. Each of the missions was completed by a control track which has the same nominal flight geometry as the first track. This allows assessing the amount of temporal decorrelation between the first and the last track. Table 2 contains a summary of the parameters which characterize the tomographic data sets.

5 PRELIMINARY RESULTS

A partially forested area of $400\ m\ x\ 1000\ m$ has been selected for tomographic processing using the HH channel of the P-band tomographic SAR data set. For simplicity, and since the selected area is relatively flat, a 3D reconstruction grid consisting of a set of horizontal layers has been chosen. The voxel spacing is $1\ m$ for both, easting and northing direction, and $1.5\ m$ in vertical direction.

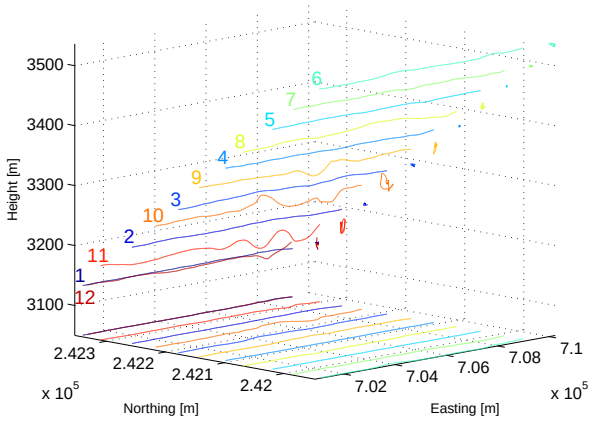

Figure 2: P-band tomographic acquisition pattern consisting of 11 flight tracks + 1 control track. The flight direction is from east to west and the sensor is left-looking. In addition to the actual flight tracks, their projections to the horizontal plane and to the northing-height plane are depicted.

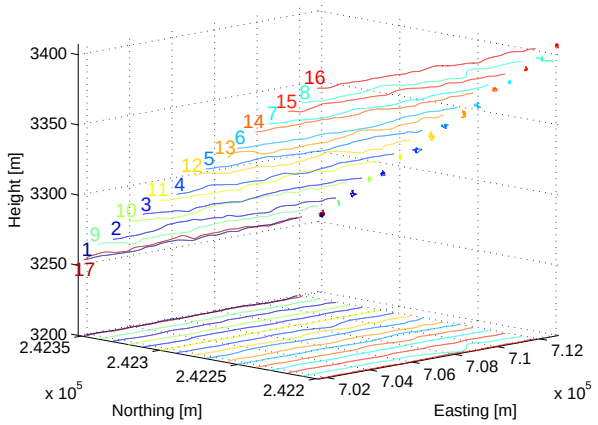

Figure 3: L-band tomographic acquisition pattern consisting of 16 flight tracks + 1 control track. The flight direction is from east to west and the sensor is left-looking. In addition to the actual flight tracks, their projections to the horizontal plane as well as to the northing-height plane are depicted.

	P-band	**L-band**
Number of flight tracks	11+1	16+1
Nominal track spacing d_n	56.6 m	14.14 m
Horizontal baselines	40 m	10 m
Vertical baselines	40 m	10 m
Synthetic aperture in normal direction L	566 m	212 m
Nominal resolution in normal direction δ_n	3 m	2 m
Approx. unambiguous height H	30 m	30 m

Table 2: Nominal parameters for tomographic processing of the P- and L-band SAR data sets.

In Fig. 4 seven tomographic slices of the imaged volume are depicted. Three of them run in south-northern direction and the other four run in west-eastern direction. For smoother visualization the data have been upsampled in the vertical direction by a factor of 2 after focusing. The tomographic slices represent the measured radar intensity values in dB. The dotted and the dashed lines indicate the height information taken from the laser DEM or DSM, respectively. In addition, the topmost horizontal layer of the volume is shown as well as an orthorectified RGB image of the same area. The RGB image was taken from the same platform during the airborne laser scanning campaign in 2003.

6 DISCUSSION AND CONCLUSIONS

High intensity values are predominantly located at the ground level within forested areas as can be seen by comparing the tomographic slices with the laser DEM/DSM. This outcome conforms with what can be expected from horizontally polarized P-band radar back-scattering of a forested area, where double-bounce scattering from the ground surface and tree trunks is a dominant scattering mechanism. However, the high intensity values are accompanied by high side lobes in the normal direction. Besides the above-mentioned limitations dictated by sparse sampling, a very probable source of these side lobes are range timing uncertainties, which still have to be eliminated by a refined geometric calibration. A system inherent problem is still given by the limited unambiguous height in the normal direction. But, it is expected that the side lobes can be much reduced by a refined phase calibration with the help of the corner reflectors.

After reprocessing of the calibrated data we intend to evaluate the quality of the TDBP-based tomographic processing (PSLR, ISLR, etc.) for all polarimetric channels. We will also quantitatively analyse whether the locations where high intensity values are detected actually conform with the occurrence of trees as indicated by the laser DEM and DSM and whether the intensity and the localization of the imaged scattering mechanisms are meaningful. The combination of all polarimetric channels of both the P-band and the L-band multi-baseline data sets is expected to give interesting insights with respect to mapping the structure of forested area by multi-baseline SAR data.

ACKNOWLEDGEMENTS

The authors would like to thank Ralf Horn, Rolf Scheiber and Martin Keller at the German Aerospace Center (DLR) for their ongoing cooperation and technical support. They would also like to thank the procurement and technology center of the Swiss Federal Department of Defense (armasuisse) for funding and supporting this work.

REFERENCES

Cumming, I. G. and Wong, F. H., 2005. Digital Processing of Synthetic Aperture Radar Data: Algorithms and Implementation. Artech House Inc., Boston, London.

Frey, O., Meier, E. and Nüesch, D., 2005. A Study on Integrated SAR Processing and Geocoding by Means of Time-Domain Backprojection. In: Proceedings of the Int. Radar Symposium, Berlin.

Frey, O., Meier, E. and Nüesch, D., 2006. An integrated focusing and calibration procedure for airborne sar data. In: Proc. of EUSAR 2006 - 6th European Conference on Synthetic Aperture Radar.

Gini, F. and Lombardini, F., 2005. Multibaseline cross-track SAR interferometry: a signal processing perspective. Aerospace and Electronic Systems Magazine, IEEE 20(8), pp. 71–93.

Guillaso, S. and Reigber, A., 2005. Polarimetric SAR Tomography (POLTOMSAR). In: Proceedings of POLINSAR'05, Frascati, Italy.

Lombardini, F. and Reigber, A., 2003. Adaptive spectral estimation for multibaseline SAR tomography with airborne L-band data. In: Geoscience and Remote Sensing Symposium, 2003. IGARSS '03. Proceedings. 2003 IEEE International, Vol. 3, pp. 2014–2016.

Moreira, A. and Huang, Y., 1994. Airborne SAR Processing of Highly Squinted Data Using a Chirp Scaling Approach with Integrated Motion Compensation. IEEE Transactions on Geoscience and Remote Sensing 32(5), pp. 1029–1040.

Nannini, M. and Scheiber, R., 2006. A Time Domain Beamforming Algorithm for SAR Tomography. In: Proc. of EUSAR 2006 - 6th European Conference on Synthetic Aperture Radar.

Reigber, A. and Moreira, A., 2000. First Demonstration of Airborne SAR Tomography Using Multibaseline L-Band Data. Geoscience and Remote Sensing, IEEE Transactions on 38(5), pp. 2142–2152.

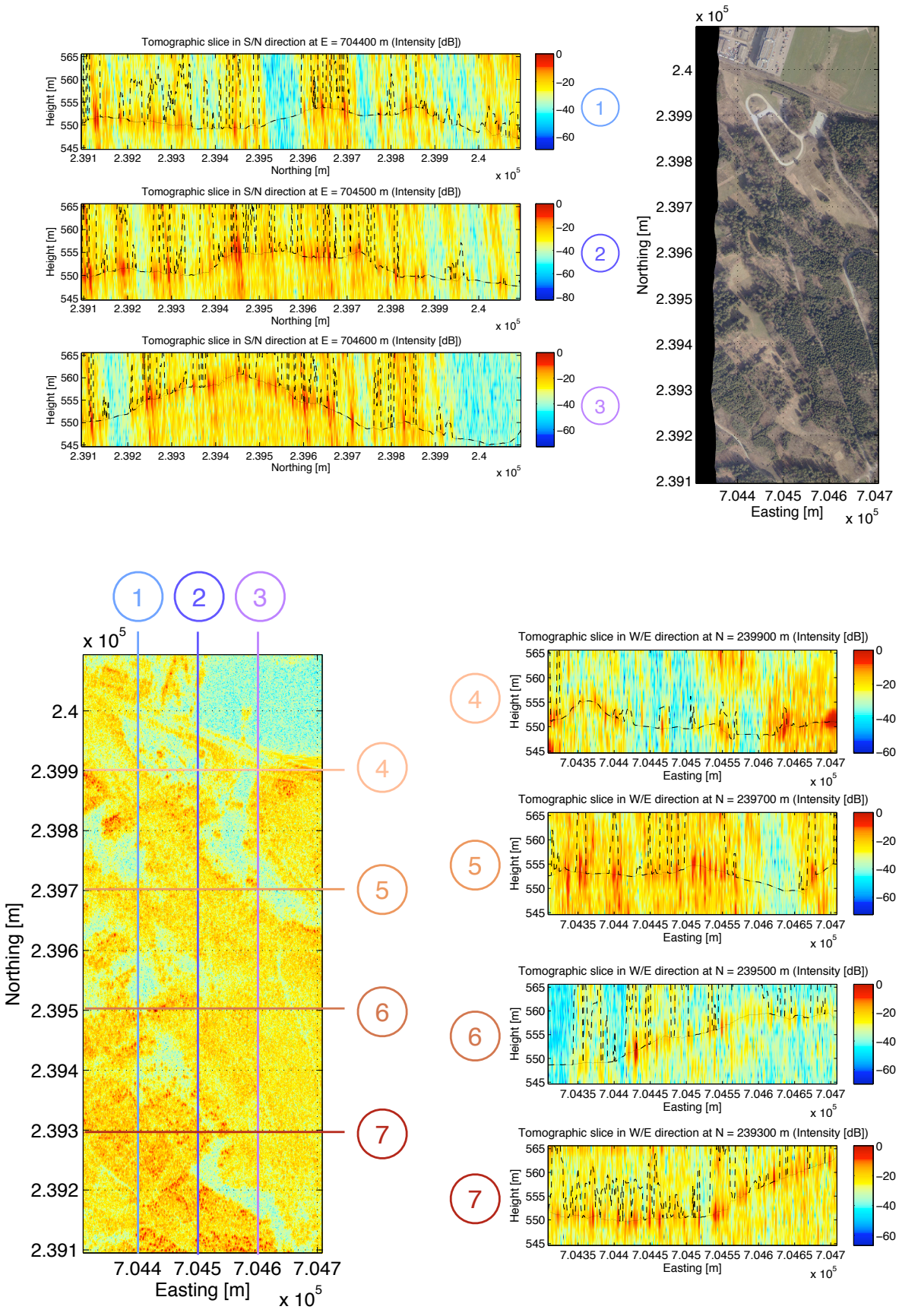

Figure 4: Tomographic slices of a forested area derived from P-band HH E-SAR data. Upper left: tomographic slices in south-northern direction. Lower left: topmost horizontal layer of the reconstruction grid. Lower right: tomographic slices in west-eastern direction. Upper right: RGB ortho-image of the same area. Dotted/dashed lines in the tomographic slices: DEM/DSM from airborne laser scanning (Falcon II, TopoSys GmbH).